J Mater Sci: Mater Med (2008) 19:3385–3397
DOI 10.1007/s10856-008-3458-6

In vitro corrosion resistance of Lotus-type porous Ni-free stainless steels

Kelly Alvarez · Soong-Keun Hyun · Shinji Fujimoto · Hideo Nakajima

Received: 5 June 2007 / Accepted: 16 April 2008 / Published online: 11 June 2008

Abstract The corrosion behavior of three kinds of austenitic high nitrogen Lotus-type porous Ni-free stainless steels was examined in acellular simulated body fluid solutions and compared with type AISI 316L stainless steel. The corrosion resistance was evaluated by electrochemical techniques, the analysis of released metal ions was performed by inductively coupled plasma mass spectrometry (ICP-MS) and the cytotoxicity was investigated in a culture of murine osteoblasts cells. Total immunity to localized corrosion in simulated body fluid (SBF) solutions was exhibited by Lotus-type porous Ni-free stainless steels, while Lotus-type porous AISI 316L showed very low pitting corrosion resistance evidenced by pitting corrosion at a very low breakdown potential. Additionally, Lotus-type porous Ni-free stainless steels showed a quite low metal ion release in SBF solutions. Furthermore, cell culture studies showed that the fabricated materials were non-cytotoxic to mouse osteoblasts cell line. On the basis of these results, it can be concluded that the investigated alloys are biocompatible and corrosion resistant and a promising material for biomedical applications.

K. Alvarez · S.-K. Hyun (✉) · H. Nakajima
The Institute of Scientific and Industrial Research, Osaka University, Ibaraki, Osaka 567-0047, Japan
e-mail: hyun23@gmail.com

S. Fujimoto
Division of Materials and Manufacturing Science, Graduate School of Engineering, Osaka University, Suita, Osaka 565-0871, Japan

1 Introduction

It is known that the properties of the passive films on stainless steels depend on the type of solution used for the corrosion tests. Stainless steels exhibit different corrosion resistance in alkaline (i.e., NaOH), neutral (i.e., NaCl, phosphate buffered saline (PBS)) and acidic (HCl, H_2SO_4) environments, since the mechanisms of formation and breakdown of the passive film are different [1].

AISI 316L stainless steel has been used as a surgical implant material for many years exhibiting a sufficient corrosion resistance under body fluids which contains Cl^- ion as well as many others components such as water, dissolved oxygen, bacteria, cells, enzymes, proteins, etc. The improved corrosion resistance of type AISI 316L stainless steel (over the common stainless steels) in a chloride environment is attributed to the addition of molybdenum which is effective in stabilizing the passive film in the presence of chlorides [2]. Recently, it has been found that nitrogen addition to the austenitic stainless steel improves the pitting corrosion resistance [3–5]. Additionally, nitrogen as an alloy component, allows a nickel content reduction in the austenitic stainless steels, very desirable consequence since the prospective of allergic reactions caused by this element.

On the other hand, porous metallic materials have attracted much attention for practical applications as heat insulating materials, porous artificial bones and dental roots, carriers for cell fixation, catalyst supports and electrodes utilizing large surface areas, vibration and acoustic energy damping materials, lightweight materials, etc.

Porous metallic biomaterials have been developed for the reconstruction of hard tissues since they provide obvious advantages over typical monolithic implants. One of these is the possibility to match the mechanical

properties to those of bone to prevent stress shielding and loosening of the implant. Metals and alloys processed to create a porous structure by means of powder metallurgy processes [6–8], solid freeform fabrication [9–11] or vapor deposition of the metal, i.e., tantalum on vitreous polymer network [12], have been shown to enhance the bone ingrowth and osseointegration [13–17]. In addition, a porous surface improves the mechanical interlocking between the host bone and the implant biomaterial [18], reinforcing the stability of the implant by biological fixation.

Nakajima and coworkers have fabricated Lotus-type porous metals possessing long cylindrical pores aligned in one direction by unidirectional solidification under pressurized hydrogen atmosphere [19–28]. The mechanical properties of Lotus-type metals are superior to that of conventional porous materials. The Young's modulus [29], yield stress [30] and ultimate tensile strength [26] in the direction parallel to the longitudinal axis of the pores decrease almost linearly with increase in porosity. Moreover, in the case of Lotus-type porous surgical grade stainless steel, when the pores are aligned perpendicular to the load direction the mechanical properties are near to the human cortical bone [31]. Therefore, Lotus-type porous stainless steel could be proposed for practical use as a biomaterial. However, propensities to pitting attack and metal ion release under simulated body fluid condition as well as cytotoxicity have not been systematically investigated until now. Corrosion performance of metallic implants is critical because it definitively affects the biocompatibility and the mechanical integrity.

In this study, electrochemical characterization was performed to study the corrosion behavior of Lotus-type porous high nitrogen nickel-free stainless steels containing different contents of chromium in a simulated biological environment. The standard corrosion parameters such as corrosion current density (i_{corr}), corrosion potential (E_{corr}), breakdown potential (E_b) and corrosion rate (C_R) were calculated from the potentiodynamic anodic polarization curves measured for Lotus-type porous stainless steels. Additionally, ion release determination by inductively coupled plasma mass spectrometry (ICP-MS) was performed in several simulated body fluid (SBF) solutions, and cytotoxicity experiments were carried out using murine osteoblasts in direct contact with the fabricated alloys.

2 Materials and methods

2.1 Specimen fabrication

Mirror polished high nitrogen Lotus-type porous nickel-free stainless steels containing different contents of chromium were employed in this study. Lotus-type porous AISI 316L stainless steels were tested also for comparison. The Lotus-type porous morphology was obtained using continuous zone melting technique, which has been described previously by the present authors [31]. Briefly, stainless steels rods were partially melted by induction heating inside a chamber pressurized with hydrogen gas and solidified by unidirectional solidification. While the rod is partially being melted is transferred downward at constant velocity and during the solidification from liquid to solid phase, gas phase separation evolves gas pores which grow aligned in one direction [28, 32]. In order to alloy the samples with nitrogen, a high temperature solution nitriding treatment was applied. The high temperature solution nitriding treatment was carried out by sealing the plate samples into a quartz tube of 20 mmϕ × 170 mm in a nitrogen atmosphere of 0.07 MPa. The encapsulated samples were heat-treated at 1,100°C for 604.8 ks and then quenched into a water bath. After this heat treatment the stainless steels samples originally of ferritic structure become austenitic. The compositions of these alloys are given in Table 1. The sample preparation for the electrochemical measurements was performed essentially as described previously [33].

2.2 Microstructural characterization

The surface morphologies of all specimens were examined by a scanning electron microscope (SEM) JEOL-JSM 6360T with acceleration energy of 15 kV. The crystalline structure of the alloys was characterized by X-ray diffraction (XRD) using a Rigaku diffractometer (model RINT 2500) with Cu Kα radiation in a scan range of 20–100° at a scan rate 4°/min.

2.3 Electrochemical measurements in SBF

2.3.1 Electrolytes

To investigate the corrosion properties of each material, in vitro electrochemical testing was performed in three

Table 1 Chemical compositions (wt.%) and pitting resistance equivalent (PRE) of tested alloys

	Fe	Cr	Mo	Ni	Mn	N	Si	P	S	C	PRE
Fe–25Cr–1N	Bal.	24.58	<0.01	<0.01	<0.01	1.08	0.03	0.002	0.001	0.002	35.38
Fe–23Cr–2Mo–1N	Bal.	22.61	1.92	<0.01	<0.01	1.05	0.04	0.002	<0.001	0.002	38.87
AISI 446-1N	Bal.	25.64	–	0.28	0.41	1.13	0.46	0.021	0.021	0.100	36.94
AISI 316L	Bal.	16.64	2.28	12.27	1.58	0.18	0.37	0.038	0.130	0.006	25.28

simulated body fluid solutions: (1) Physiological solution, contains 0.9 wt.% NaCl. (2) Phosphate-buffered saline solution without Ca and Mg ions, PBS(−). The composition of the PBS(−) solution grade 1 was (in g/l) 8 NaCl, 0.2 KCl, 0.2 KH_2PO_4, 1.15 Na_2HPO_4. After preparation, the PBS(−) solution was sterilized with a saturated water vapor at 393 K for 1.8 ks in an autoclave (KT-2322, ALP Co. Ltd., Tokyo, Japan). Freshly prepared PBS(−) solution was used for each experiment. (3) Eagle's minimum essential medium (MEM) (Sigma-Aldrich, UK) supplemented with 10 vol.% of fetal bovine serum (FBS) (INC Biomedicals, Inc., USA). This cell culture medium contains Eagles' salts in addition to 21 normal aminoacids at increased concentrations, buffered by sodium bicarbonate, without L-glutamine, ribonucleosides or deoxyribonucleosides (alpha modification).

Our rationale for selection of these simulated body fluid solutions was that the physiological solution is the simplest of biologically relevant media, phosphate buffered saline (PBS), is a standard buffer salts solution with only inorganic species that mimics the ion strength of human blood ($[Na^+] = 0.17$ M, $[K^+] = 0.01$ M, and $[Cl^-] = 0.15$ M) and the cell culture medium, MEM + FBS, is a more complex biological medium with inorganic components similar to PBS and organic acids, sugars and proteins. These solutions were chosen so that the role of the inorganic species and the organic species such as proteins and other molecules on the corrosion behavior could be determined.

2.3.2 Polarization and open circuit potential (OCP)

Potentiodynamic polarization tests were performed using a three-electrode cell system consisting of a platinum wire as the counter electrode and Ag/AgCl, 3 M KCl as the reference electrode. The electrolytes used were physiological solution (pH = 6.9), PBS(−) solution (pH = 7.6) and cell culture medium (MEM) + 10 vol.% FBS (pH = 7.4). The temperature was maintained at 37 ± 1°C during the experiments by immersing the cell in controlled temperature water bath [34]. Potentiodynamic and open circuit potential (OCP) experiments in MEM + FBS were conducted without deareation, while experiments in physiological and PBS(−) solutions were deaerated with ultra pure nitrogen gas. Before polarization the samples were kept immersed in the experimental solution for 3.6 ks at OCP. The potential was controlled using a potentiostat unit (Tohogiken Corp., model PS-07) connected to a potential and current x-y recorder (Keyence, Model GR-3500). The results were finally processed in a personal computer using a data acquisition program (Thermo Pro 3000). The potentiodynamic polarizations were performed at a scan rate of 0.333 mV s^{-1} and the scans were started at −100 mV with respect to the OCP (previously stabilized). Data collection was halted when the anodic polarization range of 1,500 mV was exceeded or the current exceeded 3 mA. Every corrosion test was repeated three times to ensure repeatability. The samples were mounted as described in an earlier work [33] and the surface area exposed to the electrolyte (about 1 cm^2) was calculated as described in [35]. The microstructure was examined after the corrosion tests using an optical microscope (Keyence Corp. VH-700) and a scanning electron microscope (SEM), JEOL-JSM 6360T. The corrosion current density was estimated by Tafel extrapolation of the polarization curve.

2.4 Metal ion leaching

Metal ion release testing was performed on porous sample disks with a diameter of 10 mm and 1 mm thickness. The disks were exposed to a defined volume of physiologic and PBS(−) solution (0.50 ml/cm^2 surface area) at 37 ± 1°C in a closed water bath for 60 days. The surfaces areas of the immersed samples were determined with the help of an image analyzer software (WinROOF version 5.0, MITANI Co.) and were estimated to be approximately 3 cm^2. Solutions without metal specimens were incubated under similar conditions and used for the blank test. Before the immersion the disks were mechanically polished with 1 μm diamond paste, giving them a mirror-like finish. After polishing the specimens were washed with acetone and de-ionized water, followed by ultrasonic cleaning in de-ionized water for 15 min and finally rinsed in de-ionized water, and dried at 403 K for 30 min. After the immersion test the sample solutions were immediately acidified by the addition of ultra pure acetic acid (PPB/Teflon. Grade 1) (Sigma-Aldrich, Japan). An elemental analysis of the leached corrosion fluid was performed by inductively coupled-plasma-mass spectroscopy (ICP-MS) (Activation Laboratories Ltd., Canada).

After the immersion test in physiological solution and PBS(−) solution, the surface morphologies of the test specimens were investigated visually as well as by scanning electron microscopy. In addition, qualitative and quantitative elemental analyses of the test specimens surfaces were carried out with an electron probe micro analyzer (EPMA), (SHIMADZU, EPMA-1600), under an accelerating voltage 15 kV. Microanalyses were performed to determine the changes and extent of corrosion of the disk faces directly exposed to the solutions.

2.5 Cell culture and sample preparation

Cytotoxicity of the solution nitrided samples was evaluated using MC3T3-E1 murine calvaria osteoblasts-like cells. The cell line was acquired from an authorized cell and gene bank (Riken Cell Bank, Ibaraki, Japan). The cells were grown and

maintained in α(minimum essential medium (α-MEM) (M.P. Biomedicals, Inc. France) supplemented with 1% kanamycin (M.P. Biomedicals, Inc. France), and 10 vol.% fetal bovine serum (FBS) (M.P. Biomedicals, Inc. France) in a humidified incubator with 95% air and 5% CO_2 at 37°C. Passaging and preparation of single cell suspensions for seeding on the metallic samples was achieved by enzymatic digestion using 0.25 vol.% trypsin, 0.02% (w/v) EDTA solution in PBS at pH 7.4. Cells counts were performed using a Tatai-type hemacytometer under an inverted microscope.

In vitro cytotoxicity was assessed by direct contact method. Disc-shaped specimens with approximate thickness of 1 mm and a diameter of 10 mm were obtained from the non-porous alloys rods using electric discharge machining. Prior to cytotoxicity testing, each specimen was ground with 2000 grit SiC paper and ultrasonically cleaned with alcohol, and then rinsed in distilled water. Subsequently, the discs were autoclaved at 121°C for 0.9 ks.

2.6 Cell proliferation, spreading and cell morphology

A total of 1,600 cells/cm^2 were inoculated to the metallic discs in 2 ml of α?minimum essential medium (α-MEM) supplemented with 10% fetal bovine serum (FBS) in a sterile collagen type IV-coated microplate with 24 well (Iwaki, Asahi Techno Glass, Japan). One test alloy sample per well was placed in direct contact with the cell monolayer. Pure Ni samples and wells without any samples were used as positive and negative controls, respectively. Cells were incubated at 37°C in a humidified 5% CO_2 atmosphere for 3- and 7-day intervals without renewal of the culture medium. After each culture period, the medium was removed and cells on the discs were immediately fixed with 70% methanol and stained with Giemsa's stain (Sigma-Aldrich). The metallic discs were rinsed with distilled water and cells were examined under optical microscope (Olympus BX-51, Olympus Optical Co., Japan) and photographed with an Nikon DS-L2 color digital camera. Control cells cultured in the collagen type IV-coated dish after staining with Giemsa solution were examined under an inverted microscope (Olympus CKX31, Olympus Optical Co., Japan). The total cell number was analyzed after staining using digital image analysis. Cell boundaries and nucleus were identified using WinROOF version 5.0 (Image analysis software, MITANI Co.). The measurements of the cell spreading area were analyzed at the different culture intervals and normalized to the maximum area available in the metallic surfaces. Cell proliferation and the assessment of extent of spreading and cell morphology assays were repeated four times. After 3 days proliferation assays, media from the cells cultured with the metallic materials were saved in quadruplicate for inductively coupled plasma (ICP) analysis.

2.7 Cell viability

Cell viability was evaluated by the modified MTT method designated WST-1 assay as indicated by the manufacturer's instructions (Roche Diagnostics GmbH, Germany). The WST-1 assay is a nonradioactive alternative to the [^{3}H] thymidine incorporation assay. The assay consists of tetrazolium salt, which is cleaved by mitochondrial dehydrogenase to form a colored compound, formazan [36]. Thus, the amount of formazan dye formed directly correlates with the number of metabolically active cells in the culture.

MC3T3-E1 cells (2×10^4 cells/well) were seeded onto non-porous metallic samples ($n = 6$) in a 48-well plate (Costar, USA) with 400 μl of α(minimum essential medium (α-MEM) plus 10 vol.% FBS. After incubation for 3 days, the cell culture medium is changed and 400 μl of fresh medium and 40 μl of WST-1 reagent was added directly to the wells containing the cell monolayer deposited over the metallic plates of Ni-free stainless steels. The wells were subjected to further incubation to facilitate the reaction between mitochondrial dehydrogenase released from viable cells and tetrazolium salt of WST-1 reagent. The incubation was carried out for 4 h at 37°C. Cell culture medium plus WST-1 was used as a negative control. The intensity of the colored compound formed (formazan dye) was then quantified using a 96-well absorbance microplate reader (Bio-Rad, Model 680) at 450 nm. The cell viability was expressed as the percentage of absorption of cells incubated in direct contact with metallic plates compared with that of cells incubated with cell culture medium alone.

2.8 Statistical analysis

Corrosion test experiments were conducted at least three times and the data shown was one representative experiment. Cytotoxicity data are presented as means ± standard deviation (SDs). Differences between two groups were statistically analyzed by Student's t-test and considered significant at $P < 0.05$. One-way ANOVA followed by Tukey's test was carried out with MatLab software package (version 6.0, MathWorks, Inc. Natick, MA, USA) to establish differences among independent samples. Differences were considered significant at $P < 0.05$.

3 Results and discussion

3.1 Microstructural characterization

The microstructures of the electrochemically characterized alloys are presented in Fig. 1. The resulting microstructure of the Ni-free stainless steel alloys consisted of coarse

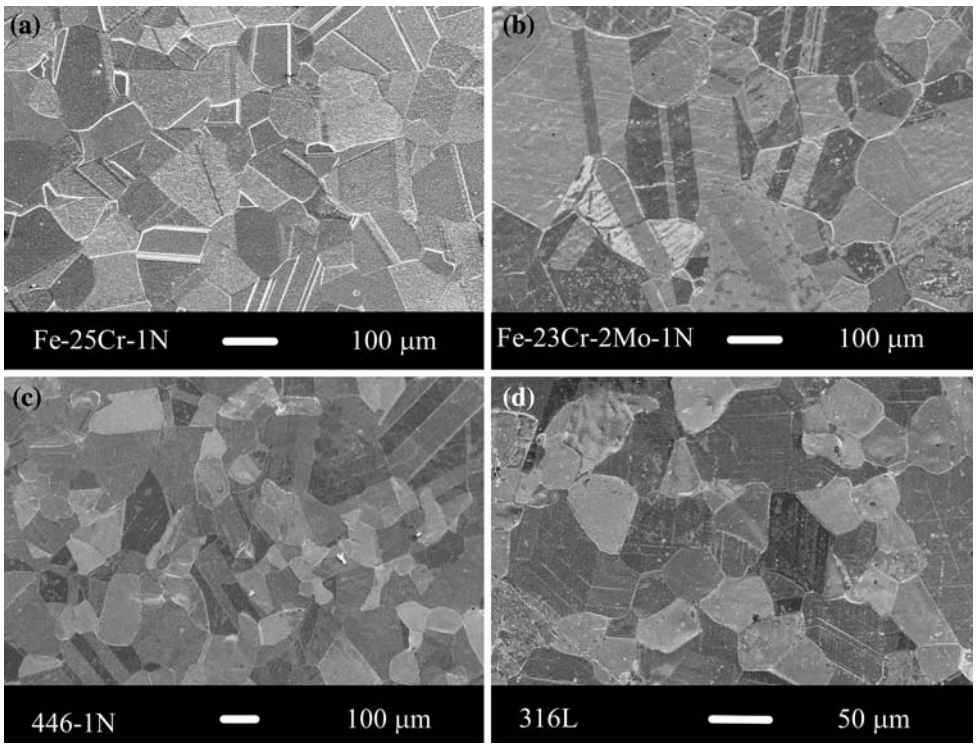

Fig. 1 SEM micrographs showing the microstructures of: (**a**) Fe–25Cr–1N, (**b**) Fe–23Cr–2Mo–1N, (**c**) AISI 446-1N and (**d**) AISI 316L. Electrolytic etch 0.1 N HCl, 1.5 V dc, 10 s

equiaxed austenite grains which contained annealing twins (Fig. 1a–c). In any of the alloys was observed grain precipitation of chromium nitrides. As a reference material AISI 316L was used; in the as-received condition its microstructure consisted of single austenitic phase (Fig. 1d). Figure 2 shows the X-ray diffraction (XRD) patterns of the fabricated Lotus-type porous Ni-free and AISI 316L stainless steels. After the solution nitriding treatment only austenite phase was observed in the profiles of the fabricated alloys. Neither CrN nor Cr_2N were identified by XRD.

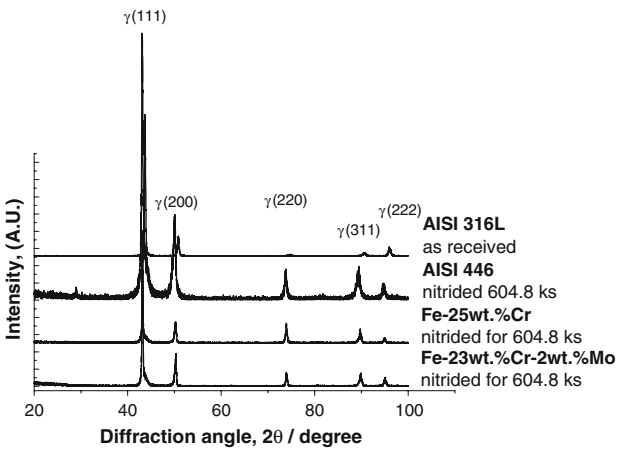

Fig. 2 X-ray diffraction patterns of the fabricated Lotus-type porous Fe–Cr–N alloys and AISI 316L stainless steel

3.2 Corrosion performance

3.2.1 Open circuit potential

Figure 3 shows the open circuit potential (OCP) versus time for the fabricated Lotus-type Ni-free stainless steels measured in the different SBF solutions. Lotus-type porous AISI 316L was also tested under the same conditions for comparison. The OCPs of the samples measured in physiologic solution are shown in Fig. 3a. Following the immersion, an abrupt OCP displacement towards less noble directions was noticed in all cases. This behavior suggests the dissolution of the oxide layer on the surface of the porous alloys as the samples are immersed in the physiologic solution. However, in the case of Fe–23Cr–2Mo–1N alloy a restoration of the passive layer can be presumed according to the asymptotical increase in the E_{corr} observed in the last stage of the measurements.

The OCPs of the samples measured in PBS(−) solution are shown in Fig. 3b. All the materials showed a tendency to reach a stable negative potential. Fe–23Cr–2Mo–1N alloy has the highest OCP after 14 h of measurement. Figure 3c shows the OCPs of the samples measured in MEM + FBS solution. The curves were recorded for 14 h with the sample immersed in aerated conditions. The overall changes in the potential are similar in shape to those of the inorganic components solutions. However, for Lotus-type porous AISI 316L sudden changes in the potential

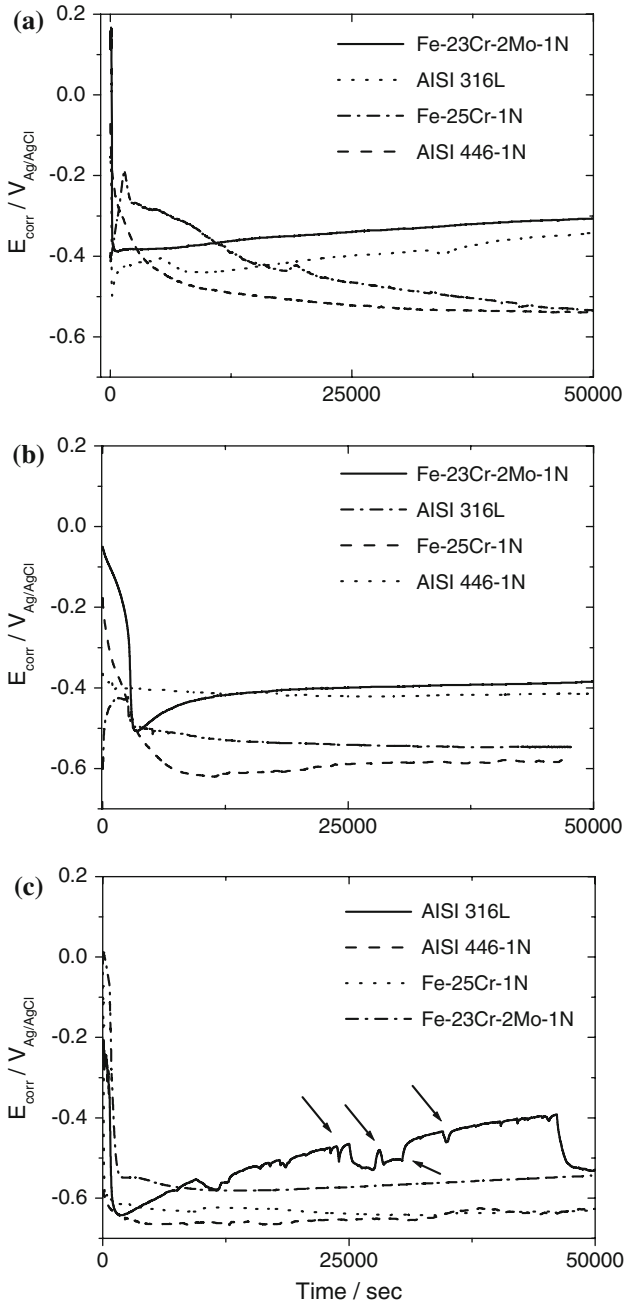

Fig. 3 Open circuit potential versus time of Lotus-type porous Fe–Cr–N alloys and AISI 316L stainless steel in (**a**) deaerated physiological solution at 37°C, (**b**) deaerated PBS(−) solution at 37°C, (**c**) aerated MEM + 10 vol.% FBS solution at 37°C

marked with arrows indicate the possibility of crevice corrosion or pitting occurring during long-term open circuit potential measurement. In MEM + 10 vol.% FBS solution, the stabilization of potential occurred at −620 mV with differences within 90 mV for the three Lotus-type porous Ni-free stainless steels. These negative stabilization potentials are an indication of extensive dissolution of passive layer in this aggressive aminoacids-containing solution.

3.2.2 Potentiodynamic polarization test

Representative anodic polarization curves of the investigated Lotus-type porous Ni-free stainless steels in the different simulated body fluids are presented in Figs. 4–6. In the polarization curves presented in Fig. 4, it can be observed that Lotus-type porous AISI 316L exhibited a low breakdown potential in physiologic solution. In contrast, no breakdown potential up to 1.2 V was found for the Lotus-type porous high nitrogen Ni-free stainless steels. It was confirmed that the nitrogen alloying of Ni-free stainless steels impedes the pitting initiation in the neutral physiological solution. In comparison of AISI 316L stainless steel, the high nitrogen Ni-free stainless steels showed evidently much lower passive current density, suggesting that the passive film formed on the Ni-free stainless steel is

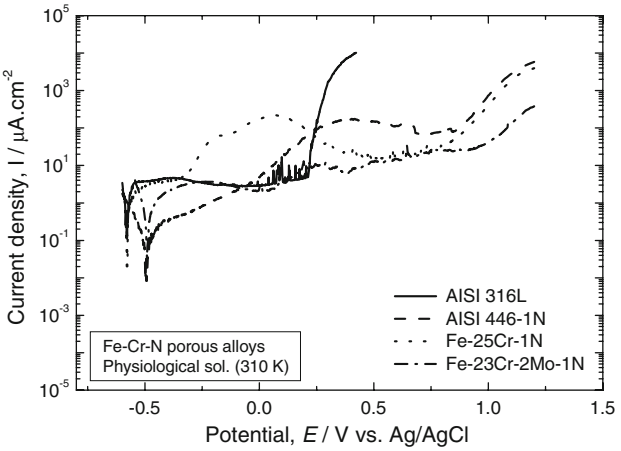

Fig. 4 Potentiodynamic polarization curves of Lotus-type porous Fe–25Cr–1N, Fe–23Cr–2Mo–1N, AISI 446-1N and AISI 316L steels measured in deaerated physiological solution at 37°C

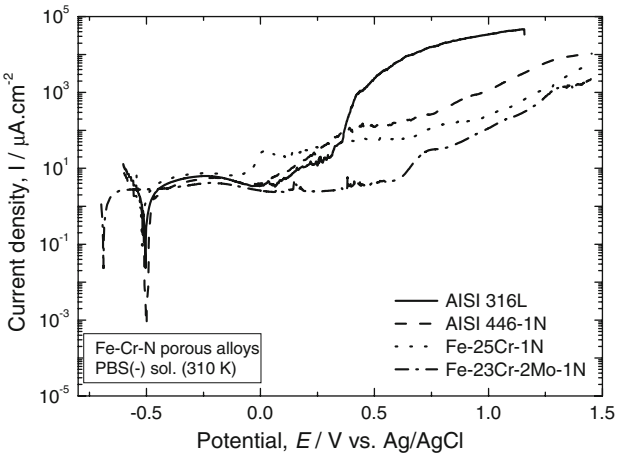

Fig. 5 Potentiodynamic polarization curves of Lotus-type porous Fe–25Cr–1N, Fe–23Cr–2Mo–1N, AISI 446-1N and AISI 316L steels measured in deaerated PBS(−) solution at 37°C

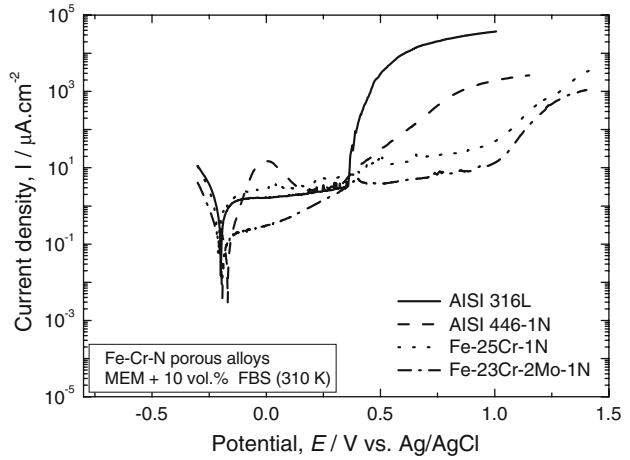

Fig. 6 Potentiodynamic polarization curves of Lotus-type porous Fe–25Cr–1N, Fe–23Cr–2Mo–1N, AISI 446-1N and AISI 316L steels in aerated MEM + 10 vol.% FBS solution at 37°C

more protective. Lotus-type porous Fe–23Cr–2Mo–1N alloy exhibited the lowest anodic current density between 0.1 and 1.2 V in physiological solution. Significant differences in the localized corrosion behavior of the Lotus-type porous samples were found also after potentiodynamic polarization test in PBS(−) solution. Figure 5 clearly illustrates the Lotus-type porous AISI 316L susceptibility for localized corrosion in PBS(−) solution. The polarization curves are very similar to Fig. 4 although for AISI 316L the current density is one order of magnitude lower in PBS(−) solution than in physiological solution. Additionally, the breakdown potential of AISI 316L in PBS(−) solution resulted to be 100 mV higher than in physiological solution. This is perhaps due to the slightly lower chloride ion concentration of PBS(−) solution and also to its buffer action. In general, during the pit propagation the local environment is acidified by the hydrolysis of the dissolving metal, and the metal inside the pit is maintained in an actively dissolving state. However, PBS(−) solution might stabilize the pH at the pit surface contributing with the repassivation. In Fig. 6 the polarization curves of the solution nitrided porous samples measured in MEM + 10 vol.% FBS are shown. Under these conditions, AISI 446-1N and AISI 316L show the typical behavior of a material prone to pitting corrosion when the applied potential is higher than a threshold. Due to the presence of aminoacids and higher salts concentrations the pitting occurred in AISI 446-1N at a low potential value (about 400 mV Ag/AgCl). The results presented in Tables 2, 3 and 4 show the outstanding pitting corrosion resistance of Lotus-type porous Ni-free stainless steels in the inorganic artificial body fluids against AISI 316L stainless steel. Statistical analysis showed that the corrosion rate of Lotus-type porous Ni-free stainless steels resulted to be lower

Table 2 Corrosion potential, breakdown potential and passive current density of the samples measured in anodic polarization curves at 37°C in physiological solution

Specimen	E_{corr} mV vs. Ag/AgCl	E_b mV vs. Ag/AgCl	Passive current density at 0.5 V (μA/cm^2)	Corrosion rate (C_R) mm/y × 10^2
AISI 316L	−578	200	10100	3.00
AISI 446-1N	−498	–	151	1.02
Fe–25Cr–1N	−559	–	18	1.49
Fe–23Cr–2Mo–1N	−492	–	13	1.16

Table 3 Corrosion potential, breakdown potential and passive current density of the samples measured in anodic polarization curves at 37°C in PBS(−) solution

Specimen	E_{corr} mV vs. Ag/AgCl	E_b mV vs. Ag/AgCl	Passive current density at 0.5 V (μA/cm^2)	Corrosion rate (C_R) mm/y × 10^2
AISI 316L	−504	300	1412	2.30
AISI 446-1N	−509	–	127	0.83
Fe–25Cr–1N	−519	–	59	1.18
Fe–23Cr–2Mo–1N	−689	–	4	0.97

Table 4 Corrosion potential, breakdown potential and passive current density of the samples measured in anodic polarization curves at 37°C in MEM + 10 vol.% FBS solution

Specimen	E_{corr} mV vs. Ag/AgCl	E_b mV vs. Ag/AgCl	Passive current density at 0.5 V (μA/cm^2)	Corrosion rate (C_R) mm/y × 10^2
AISI 316L	−201	360	2874	2.22
AISI 446-1N	−169	400	31	1.98
Fe–25Cr–1N	−210	–	19	1.40
Fe–23Cr–2Mo–1N	−194	–	4	0.56

than Lotus-type porous AISI 316L under the various test conditions. The results obtained in MEM + 10 vol.% FBS (Table 4) indicate a very good performance of Lotus-type porous Fe–25Cr–1N and Fe–23Cr–2Mo–1N alloys.

The corrosion resistance of nitrogen alloyed austenitic steels is mainly determined by the contents of chromium, molybdenum, and nitrogen. The Pitting Resistance Equivalent (PRE) parameter establishes a ranking of resistance o pitting corrosion. Various formulations of the kind PRE = %Cr + 3.3%Mo + X%N (X varying from 8 to 30) have been proposed [37–40]. Table 1 shows the PRE numbers of the investigated alloys. The PRE numbers were calculated according to the following formula due to Haruki et al. [40]:

$$\mathrm{PRE} = \%\mathrm{Cr} + 3\%\mathrm{Mo} + 10\%\mathrm{N} \quad (1)$$

The above formulation of PRE was chosen, among the different ones, because it was obtained after experiments with high nitrogen and conventional austenitic stainless steels in a neutral chloride environment.

Obviously, the tested Ni-free stainless steels show similar performances in neutral solutions containing chloride ions because their PRE numbers are similar (35.38–38.87). This also explain why AISI 316L exhibited a very low breakdown potential (PRE = 25.28), while in the fabricated Ni-free stainless steels pitting attack never occurred at potentials values up to 1.2 V vs. Ag/AgCl. Interestingly, Fe–23Cr–2Mo–1N alloy which has the highest PRE value (38.87), exhibited lower anodic current values within a wide range of potentials. This superior behavior is maintained even in the MEM + 10 vol.% FBS electrolyte.

The excellent localized corrosion resistance of the Lotus-type porous high nitrogen Ni-free stainless steels is not surprising, since previously, the pitting corrosion resistance of these porous alloys was evaluated in severe electrochemical test conditions and showed very good performance when exposed in a very aggressive environment [33].

The surface morphology after pitting corrosion test of the Lotus-type porous high nitrogen Ni-free stainless steels for pitting was confirmed by SEM. Figures 7, 8 and 9 show the SEM photographs of the different corroded surfaces after the potentiostatic polarization test in physiological solution, PBS(−) solution, and MEM + 10 vol.% FBS solution. Pitting corrosion was not observed for all Lotus-type porous high nitrogen Ni-free stainless steels after the potentiodynamic polarization tests in the simulated body fluids. Figures 7d, 8d and 9d show the nature of the pitting attack observed in AISI 316L. Figure 9c shows very small perforated pits found in the surface of AISI 446-1N after the polarization test in MEM + 10 vol.% FBS solution. The surface of the AISI 316L corroded in the differently simulated body fluids reveals the presence of many open perforated pits in the surroundings of the pores (Figs. 7d, 8d and 9d). Thus, it is evident that SEM results are in good agreement with the results of the potentiodynamic polarization curves. The corrosion resistance of Lotus-type porous AISI 316L is very low even in these neutral physiological environments.

3.3 Metal ion leaching

Metal release from implants or devices in contact with human fluids or tissue has concerned surgeons because their patients have exhibited allergies attributable to specific metals (e.g., nickel). For this reason, metal ion release analysis is necessary in order to provide an order-of-magnitude estimate of released metals at least in simulated physiological environment. Table 5 shows the results of the released element concentrations from the investigated alloys obtained by ICP-MS. Metal concentrations of the

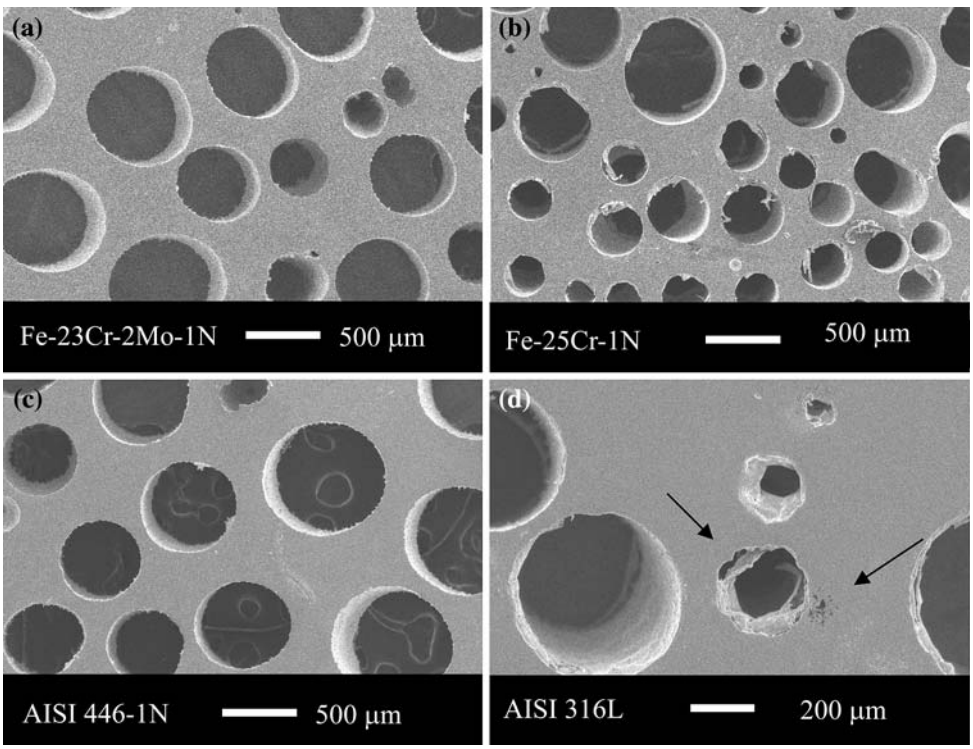

Fig. 7 SEM photographs of the investigated porous alloys after the polarization in physiological solution at 37°C. (**a**) Fe–23Cr–2Mo–1N, (**b**) Fe–25Cr–1N, (**c**) AISI 446-1N, (**d**) AISI 316L

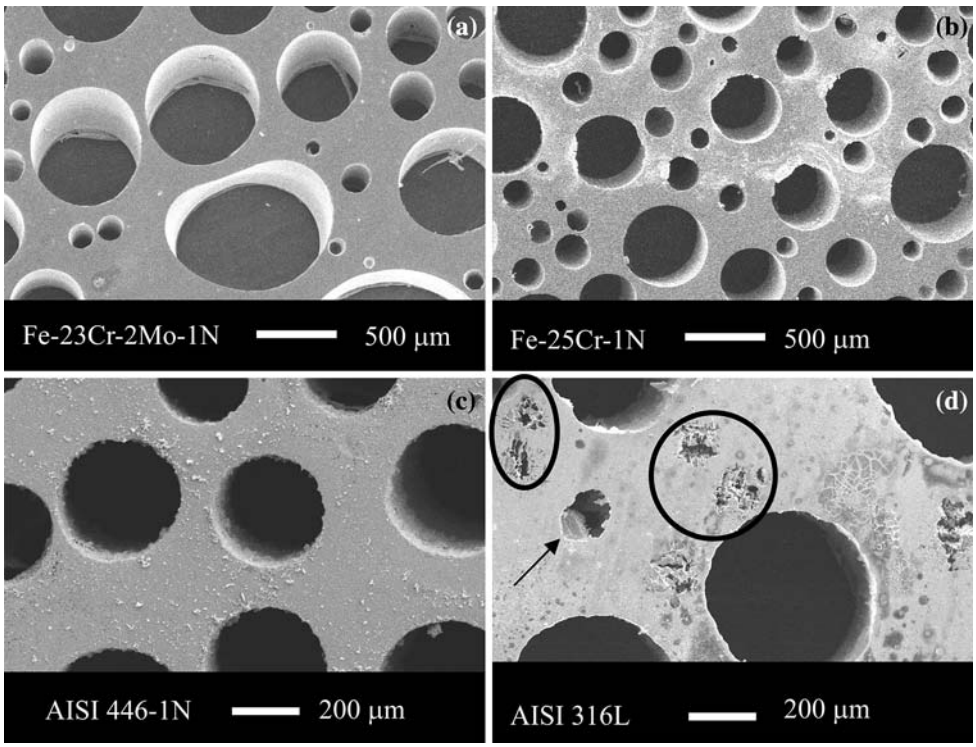

Fig. 8 SEM photographs of the investigated porous alloys after the polarization in PBS(−) solution at 37°C. (**a**) Fe–23Cr–2Mo–1N, (**b**) Fe–25Cr–1N, (**c**) AISI 446-1N, (**d**) AISI 316L

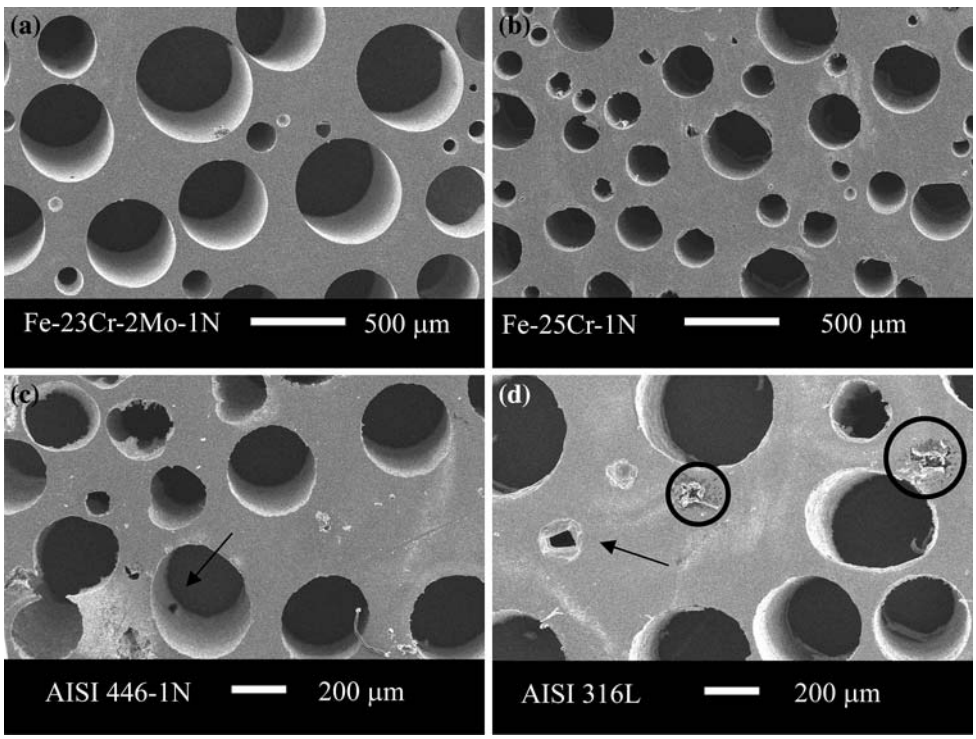

Fig. 9 SEM photographs of the investigated porous alloys after the polarization in MEM + 10 vol.% FBS solution at 37°C. (**a**) Fe–23Cr–2Mo–1N, (**b**) Fe–25Cr–1N, (**c**) AISI 446-1N, (**d**) AISI 316L

reference samples were subtracted from those of the exposed solution samples to obtain the amounts of released metals. The predominant elements released from the alloys were Al, Mn, Cr, Fe, Mo and Ni. In general, the elements detected were of the same order of magnitude as that in the blanks. A comparison of metal release from the investigated porous alloys in the different SBF solutions, show that Fe is preferentially released from all the samples,

Table 5 Amounts of metal ions released in ppb from the investigated alloys in physiological, PBS(−) and MEM + FBS solution measured by ICP-MS[a]

Element	Physiologic solution				PBS(−) solution				MEM + FBS solution[b]			
	Fe–23Cr–2Mo–1N	Fe–25Cr–1N	AISI 446-1N	AISI 316L	Fe–23Cr–2Mo–1N	Fe–25Cr–1N	AISI 446-1N	AISI 316L	Fe–23Cr–2Mo–1N	Fe–25Cr–1N	AISI 446-1N	AISI 316L
Al (μg/l)	<2	<2	<2	<2	<2	<2	<2	<2	<2	<2	<2	<2
Mn (μg/l)	<0.1	<0.1	<0.1	<0.1	0.1	0.1	0.1	0.2	0.2	0.1	0.3	0.1
Cr (μg/l)	<0.5	<0.5	<0.5	<0.5	<0.5	<0.5	<0.5	<0.5	5	5	6	3
Fe (μg/l)	35	22	60	52	60	60	56	50	124	119	110	98
Mo (μg/l)	0.5	<0.1	<0.1	0.6	0.3	<0.1	<0.1	0.5	0.1	<0.1	<0.1	0.2
Ni (μg/l)	<5	<5	<5	9	<5	<5	6	11	<5	<5	<5	<5

[a] The detection limits for the elements were 2 μg/l Al, 0.1 μg/l Mn, 0.5 μg/l Cr, 10 μg/l Fe, 0.1 μg/l Mo, and 5 μg/l Ni

[b] Discs were incubated in culture medium (MEM + FBS) for 3 days at 37°C

while the rest of the alloy constituents are practically below of the detection limit, with the exception of Ni, which was leached by the AISI 446-1N and AISI 316L in small proportions in PBS(−) solution. The quantities of metals released into MEM + 10 vol.% FBS solution were higher than those in physiologic solution and PBS(−) solution, even though the duration of the immersion test in the cell culture medium was just 3 days. According to several researches [41, 42] it has been found that the release rate for metal ions is higher during the early part of the exposure and decreases during the subsequent exposure time. On the other hand, cell culture medium is a significant source of metal ions such as Fe, Cr, Zn, etc. this could interfere one way or another in the results. The test coupons after the immersion test were examined with scanning electron microscopy for visible indications of pitting corrosion. Microscopic examination revealed no evidence of pitting after immersion of the investigated samples in physiological, PBS(−) and MEM + 10 vol.% FBS solutions.

3.4 EPMA analysis after the immersion test

The visual inspection of the specimens after the immersion test in physiological solution shows that for AISI 446-1N and Fe–23Cr–2Mo–1N about 50% of the surface appears to be covered with a white type of layer, which cannot be removed by repeated washing in water. In the case of Fe–25Cr–1N the cover layer extended about 30% of the surface and was orange color. The EPMA analysis done on these deposits revealed the presence of Fe, Cr, N and O peaks besides some minority elements such as Si, P, S, Al and Cu. The oxygen peak obviously indicates that this layer is an oxide or hydroxide layer that formed after the immersion in physiological solution.

The appearance of the test specimens immersed in PBS(−) was also coated with some deposits firmly adhered to the substrates. The EPMA analysis of these deposits revealed K and P peaks and indicate that the precipitates are highly enriched in K and P.

3.5 In vitro cytocompatibility studies

Cytotoxicity testing of surgical implants materials is an important way to verify their biocompatibility. The quantitative results of the proliferation test obtained with the image analysis software are presented in Fig. 10. The cells cultured for 7 days multiplied actively on the four stainless steel surfaces compared to those cultured for 3 days. After each culture period, cells grown on stainless steel surfaces displayed a significantly ($P < 0.05$) lower proliferation rate than the cells cultured on Type IV collagen-coated cell culture dish. One-way ANOVA showed no statistically

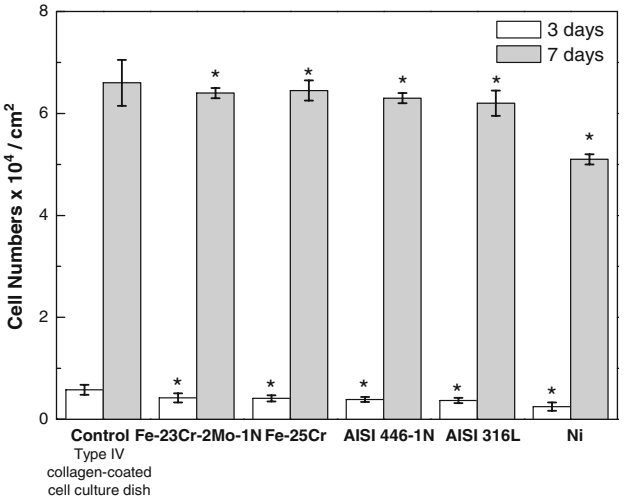

Fig. 10 Proliferation rates after 3 and 7 days in direct contact with the evaluated metallic materials with respect to the control cultures grown on Type-IV collagen-coated cell culture dish (100%); means ± SDs; significant difference: $*P < 0.05$ compared to control, $n = 4$

significant difference for the cell numbers of the four stainless steel samples after 3 and 7 days of culturing ($P > 0.05$). In the case of pure Ni samples after 7 days in culture, the cell numbers were significantly smaller than that of the four stainless steel samples and negative controls ($P < 0.05$). While in the stainless steel surfaces cells proliferated forming multilayers after 7 days of culture, in the pure Ni samples was observed the formation of randomly located multilayer cell nodules, indicating that the spreading was scarce and not uniform.

Morphology of adherent cells after 3 days incubation period is shown in Fig. 11. Microscopic analysis of the cell monolayers revealed that there were no notable differences in cell morphology between the type IV collagen cell culture dish (Fig. 11C) and the stainless steels (Fig. 11a–h). The body of osteoblasts has a mean size of 15 μm and many of them developed arm-like cytoplasmatic extensions with lengths up to 25 μm. MC3T3-E1 cells seemed to adhere tightly to surfaces under high magnification (750× magnification) (Fig. 11e, f, g and h) in accordance with the flattened morphology surrounded by cytoplasmatic prolongations. MC3T3-E1 osteoblasts cells proliferated uniformly on the surface of Ni-free stainless steels under optical microscope (100× magnification) (Fig. 11a–d). Microscopic analysis of the cells cultured on pure Ni samples revealed that the cell morphology was altered. Cells grown on pure Ni exhibited reduced cytoplasmatic area and also abnormally large cells (giant cells) were observed in both cultivation periods (Fig. 12).

After 3 days of culture, the MC3T3-E1 cellular spreading was good in all the evaluated stainless steel surfaces but not as extensive as in the cell culture dish treated with type IV collagen, and after 7 days of culture, osteoblasts were evenly spread covering the entire available stainless steel surfaces. Statistically significant differences between the average area of cells cultivated on the Ni-free stainless samples and AISI 316L samples was not observed.

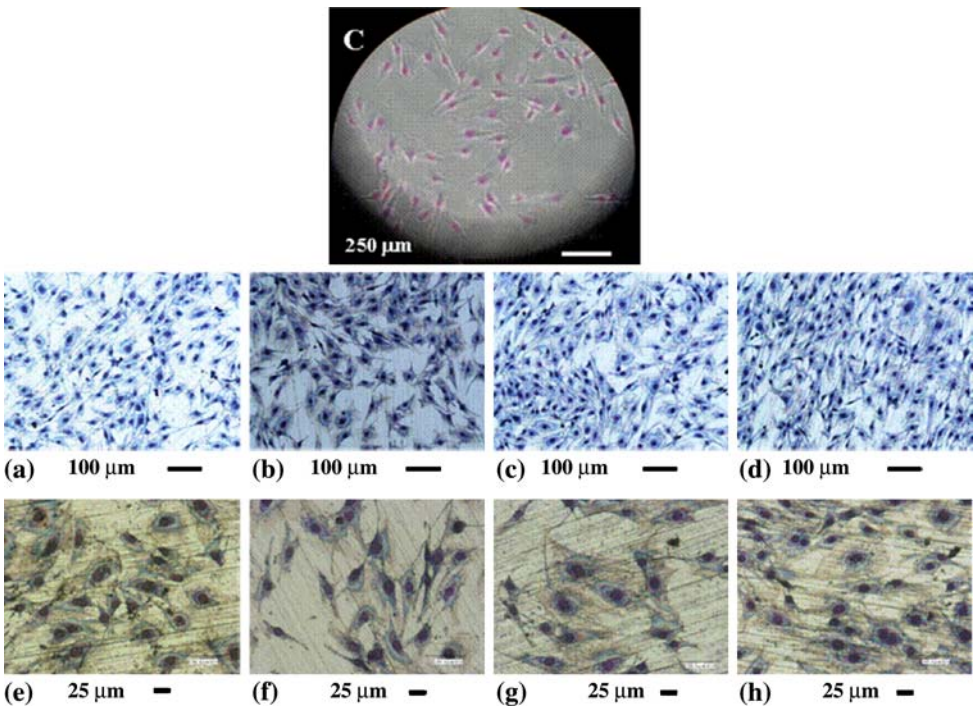

Fig. 11 Representative optical microscopy images of spread MC3T3-E1 osteoblasts cells after 3 days of direct cultivation on (**C**) Type-IV collagen-coated cell culture dish, (**a**) and (**e**) Fe–23Cr–2Mo–1N, (**b**) and (**f**) Fe–25Cr–1N, (**c**) and (**g**) AISI 446-1N, (**d**) and (**h**) AISI 316L. MC3T3-E1 cells are approaching confluence and display normal morphology. Original magnification: (**C**) 15×, (**a–d**) 100×, (**e–h**) 750×

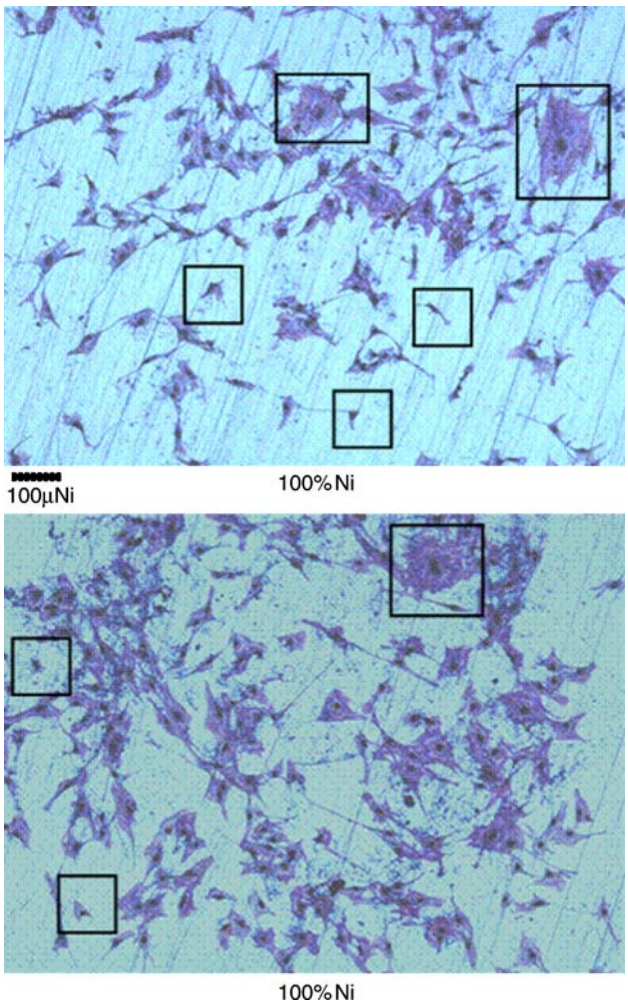

Fig. 12 Optical microscopy images of MC3T3-E1 osteoblasts cells grown on pure Ni samples. A higher frequency of reduced cyoplasmatic area cells and giant cells were observed

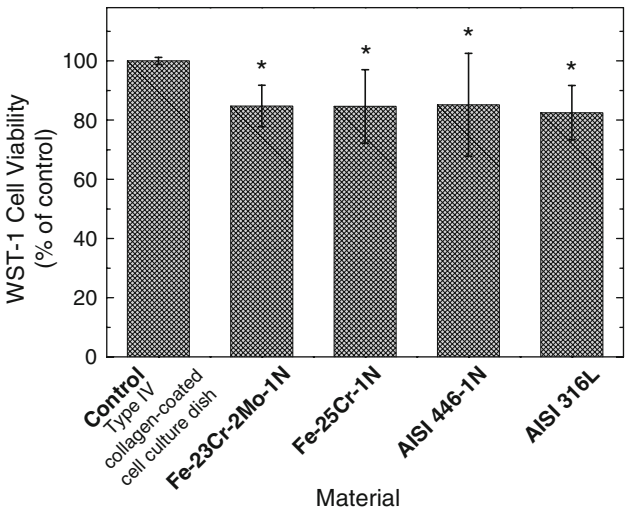

Fig. 13 Quantitative cell viability assessed using WST-1 assay by measuring the mitochondrial dehydrogenase with respect to the control cultures grown on Type-IV collagen-coated cell culture dish (100%); means ± SDs; significant difference: $*P < 0.0005$, compared to control, $n = 6$

Figure 13 shows the quantitative cell viability results measured using the WST-1 assay. As expected, the metabolic activity of cells grown on the metallic substrates was reduced compared to the control. Analysis of variance of the variability data demonstrated that the control cells had the statically highest mean absorbance values (highest viability). The number of living cells was approximately 80% ($P < 0.0005$) of control for all the investigated samples. After the exposure period of 72 h, no statistically significant difference was observed between Ni-free stainless steels and AISI 316L ($P > 0.05$). This behavior of Ni-free stainless steels and AISI 316L was rather unexpected since the nickel content in AISI 316L possesses a significant cytotoxicity potential. Nevertheless, according to our results the levels of iron, chromium and nickel ions released into SBF solutions during 60 days are significantly low (Table 5). In short periods of time these levels on ion release per se might not induce severe cytotoxic effects. However, in extended periods of time the released nickel ions may act as cofactors or inhibitors in enzymatic processes involved in protein synthesis and cell replication [43], disrupt intracellular organelles, alter cell morphology, and decrease cell numbers [44–48]. To observe more significant differences in the behavior of the cells after contact with different materials metabolic changes (structural proteins, apoptosis, etc.) need to be evaluated.

In summary, Lotus-type porous Ni-free stainless steels developed for biomedical applications is shown here to have a high performance concerning its corrosion resistance. The susceptibility to pitting corrosion is very low in SBF solutions and the corrosion rate is lower than AISI 316L. Furthermore, the fabricated Lotus-type porous Ni-free stainless steels exhibited low cytotoxicity in contact with bone forming cells. The levels of metallic ions released into SBF solutions were too low to induce severe cytotoxic effects. These results speak in favor of the utilization of high nitrogen Ni-free stainless steel over AISI 316L for surgical implants particularly in the case of persons with nickel sensitization. However, in vitro testing is only a preliminary screening for biocompatibility. Therefore, potential clinical applications of Lotus-type porous Nickel-free stainless steel must be evaluated in long term in vivo studies.

4 Conclusion

The results of the corrosion testing of high nitrogen Lotus-type porous Ni-free stainless steels in physiological saline

solution, PBS(−) solution and cell culture medium (MEM + 10 vol.% FBS) allow the following conclusions:

1. Lotus-type porous Ni-free stainless steels showed superior localized corrosion resistance than the commonly used AISI 316L stainless steel and can be recommended as an appropriate stainless steel meant for people with Ni sensitization.
2. Although the vulnerability of porous materials to pitting corrosion is well known, total immunity to localized corrosion under simulated body fluid solutions was obtained in Lotus-type porous Ni-free stainless steels by alloying with approximately 1 wt.% of nitrogen.
3. The corrosion rate of Lotus-type porous Ni-free stainless steels is 1/2 to 1/3 lower than Lotus-type porous AISI 316L stainless steel.
4. The best-localized corrosion resistance in this study was found to be Lotus-type porous Fe–23Cr–2Mo–1N stainless steel.
5. Cell culture studies showed that the fabricated materials were non-cytotoxic to mouse osteoblasts cell line.

Acknowledgements Support for this work was provided by "Priority Assistance for the Formation of Worldwide Renowned Centers of Research for the 21st Century COE Program (Project: Centre of Excellence for Advanced Structural and Functional Materials Design)'' from the Ministry of Education, Sports, Culture, Science and Technology of Japan (MEXT). K. Alvarez was supported by a scholarship from the Japanese Government (MONBUKAGAKUSHO) and really acknowledges MEXT, for the financial support for this research. The authors thank Ritsuko Nakatsu for her assistance in cell culture experiments.

References

1. C.P. Dillon, *Corrosion Resistance of Stainless Steels* (Marcel Dekker, Inc., New York, 1995), p. 258
2. K.H.W. Seah, X. Chen, Corros. Sci. **34**, 1841 (1993)
3. A. Fossati, F. Borgioli, E. Galvaneto, T. Bacci, Corros. Sci. **48**, 1513 (2006)
4. A. Di Schino, M. Barteri, J.M. Kenny, J. Mater. Sci. **38**, 3257 (2003)
5. A. Rechsteiner, M. Speidel, in *Proceedings of the 1st European Stainless Steel Conference*, vol. 2 (Florence, 1997), p. 107
6. C. Greiner, S.M. Oppenheimer, D.C. Dunand, Acta Biomater. **1**, 705 (2005)
7. C.S.Y. Jee, N. Özgüven, Z.X. Guo, J.R.G. Evans, Metall. Mater. Trans. **31B**, 1345 (2000)
8. I.H. Oh, N. Nomura, N. Masahi, S. Hanada, Scripta Mater. **49**, 1197 (2003)
9. M. Bram, Adv. Eng. Mater. **2**, 196 (2000)
10. C.E. Wen, Y. Yamanda, K. Shimojima, Y. Chino, T. Asahina, M. Mabuchi, Eur. Cells Mater. **1**, 61 (2001)
11. J.P. Li, S.H. Li, K. de Groot, P. Layrolle, Key Eng. Mater. **218**, 51 (2002)
12. J.D. Bobyn, G.J. Stackpool, S.A. Hacking, M. Tanzer, J.J. Krygier, J. Bone Joint Surg. Br. **81**(5), 907 (1999)
13. H.U. Cameron, R.M. Pilliar, I. Macnab, J. Biomed. Mater. Res. **10**, 295 (1976)
14. J.D. Bobyn, K.-K. Toh, S.A. Hacking, M. Tanzer, J.J. Krigier, J. Arthoplasty **14**, 347 (1999)
15. J. Galante, W. Rostoker, R. Lueck, R.D. Ray, J. Bone Joint Surg. [Am.] **53A**, 101 (1971)
16. X. Zhang, R.A. Ayers, K. Thorne, J.J. Moore, F. Schowengerdt, Biomed. Sci. Instrum. **37**, 463 (2001)
17. X. Zou, H. Li, M. Bunger, N. Egund, M. Lind, C. Bunger, Spine J **4**, 99 (2004)
18. B.J. Story, W.R. Wagner, D.M. Gaisser, S.D. Cook, A.M. Rust-Dawicki, Int. J. Oral Maxillofac. Implants **13**(6), 749 (1998)
19. S. Yamamura, H. Shiota, K. Murakami, H. Nakajima, Mater. Sci. Eng. **A318**, 137 (2001)
20. S.K. Hyun, H. Nakajima, in *Cellular Materials and Metal Foaming Technology*, ed. by J. Banhart, M.F. Ashby, N.A. Fleck (MIT Verlag Publishers, Bremen, 2001), pp. 181–186
21. S. Yamamura, K. Murakami, H. Shiota, H. Nakajima, in *Cellular Materials and Metal Foaming Technology*, ed. by J. Banhart, M.F. Ashby, N.A. Fleck (MIT Verlag Publishers, Bremen, 2001), pp. 425–428
22. T. Ikeda, M. Tsukamoto, H. Nakajima, Mater. Trans. **43**, 2678 (2002)
23. S.K. Hyun, H. Nakajima, Mater. Trans. **43**, 526 (2002)
24. H. Nakajima, S.K. Hyun, T. Ikeda, Acta Tech. Napocensis **45**, 3 (2002)
25. S.K. Hyun, K. Murakami, H. Nakajima, Mater. Sci. **A299**, 241 (2001)
26. S.K. Hyun, K. Murakami, H. Nakajima, in *Cellular Materials and Metal Foaming Technology*, ed. by J. Banhart, M.F. Ashby, N.A. Fleck (MIT Verlag Publishers, Bremen, 2001), pp. 421–424
27. T. Ikeda, T. Aoki, H. Nakajima, Bull. Iron Steel Inst. Jpn. **90**, 9 (2004)
28. T. Ikeda, T. Aoki, H. Nakajima, Metal Mater. Trans. **36A**, 77 (2005)
29. M. Tane, T. Ichitsubo, S.K. Hyun, H. Nakajima, J. Mater. Res. **20**, 135 (2005)
30. M. Tane, T. Ichitsubo, H. Nakajima, S.K. Hyun, M. Hirao, Acta Mater. **52**, 5195 (2004)
31. K. Alvarez, K. Sato, S.K. Hyun, H. Nakajima, Mater. Sci. Eng. C **28**, 44 (2008)
32. H. Nakajima, *Cellular Metals and Polymers 2004* (Trans. Tech. Publications Switzerland, 2005), p. 7
33. K. Alvarez, S.K. Hyun, H. Tsuchiya, S. Fujimoto, H. Nakajima, Corros. Sci. **50**, 183 (2008)
34. Designation: F746. *Standard Test Method for Pitting or Crevice Corrosion of Metallic Surgical Implant Materials. Annual Book of ASTM Standards*, vol. 13.01 (American Society for Testing and Materials, Philadelphia, PA, 1999), p. 202
35. M. Fuseya, T. Nakahata, S.K. Hyun, S. Fujimoto, H. Nakajima, Mater. Trans. **47**(9), 2229 (2006)
36. M. Ishiyama, H. Tominaga, M. Shiga, K. Sasamoto, Y. Ohkura, K. Ueno, Biol. Pharm. Bull. **19**, 1518 (1996)
37. J.E. Truman, *UK Corrosion 87* (Brighton, 1987), p. 111
38. G. Herbsleb, Werkst. Korros. **33**, 334 (1982)
39. G. Rondelli, B. Vicentini, A. Cigada, Mater. Corros. **46**, 628 (1995)
40. N. Haruki, T. Kimura, M. Kuroda, H. Miyuki, T. Kudo, in *Proceedings Stainless Steels '91*, vol. 2 (Chiba, 1991), p. 1175
41. W. He, J. Pan, I. Odnevall Wallinder, C. Leygraf, *Report of a Follow-up Study of Corrosion/Dissolution of Stainless Steels in a Range Synthetic Biologic Media*, Eurofer Internal Report (2002)
42. G. Herting, I. Odnevall Wallinder, C. Leygraf, Corros. Sci. **48**, 2120 (2006)
43. G.A. Gristina, Science **237**, 1588 (1987)
44. T.A. Rae, J. Bone Joint Surg. **57**(B), 444 (1975)
45. N. Jacobsen, Scand. J. Dent. Res. **85**, 567 (1977)
46. H. Kawahara, Int. Endod. **J 33**, 350 (1983)
47. E.J. Evans, I.T. Thomas, Biomaterials **7**, 25 (1986)
48. R.G. Craig, C.T. Hanks, J. Dent. Res. **69**, 1539 (1990)